CRYSTAL GROWTH & DESIGN

Article

Cite This: Cryst. Growth Des. 2019, 19, 3694−3703

pubs.acs.org/crystal

Effect of Substituent Size and Isomerization on the Polymorphism of 2-(Naphthalenylamino)-benzoic Acids

Yuting Liu,[†] Mingtao Zhang,[‡] Danrui Xu,[†] Sean Parkin,[§] Tonglei Li,[∥] Conggang Li,[⊥] Zhaoyong Yang,[#] Faquan Yu,*[,†] and Sihui Long*[,†]

[†]Key Laboratory for Green Chemical Process of Ministry of Education, Hubei Key Laboratory of Novel Reactor and Green Chemical Technology, Hubei Engineering Research Center for Advanced Fine Chemicals, School of Chemical Engineering and Pharmacy, Wuhan Institute of Technology, 206 First Road Optics Valley, East Lake New Technology Development District, Wuhan, Hubei 430205, China

[‡]Computational Center for Molecular Science, College of Chemistry, Nankai University, Tianjin, China

[§]Department of Chemistry, University of Kentucky, Lexington, Kentucky 40506, United States

[∥]Department of Industrial and Physical Pharmacy, Purdue University, West Lafayette, Indiana 47907, United States

[⊥]Wuhan Institute of Physics and Mathematics, Chinese Academy of Sciences, Wuhan, Hubei, China

[#]Key Laboratory of Biotechnology of Antibiotics, Ministry of Health, Institute of Medicinal Biotechnology, Chinese Academy of Medical Sciences & Peking Union Medical College, Beijing 100050, China

Supporting Information

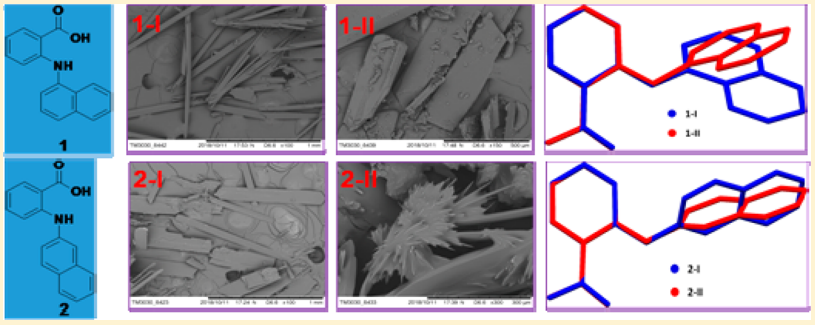

ABSTRACT: To probe the effect of substituent size and isomerization on the polymorphism of fenamic acid (FA) derivatives, we synthesized two FA analogues, namely, 2-(naphthalen-1-ylamino)-benzoic acid and 2-(naphthalen-2-ylamino)-benzoic acid (NBAs), and investigated their polymorphism. Contrary to the lack of polymorphism in FA, we discovered two crystal forms (**1-I**, **1-II**, **2-I**, and **2-II**) for each of the two compounds. We characterized the two polymorphic systems with single-crystal X-ray diffraction, powder X-ray diffraction, and infrared and Raman spectroscopy, and observed certain structural similarities between **1-I** and **2-I**. The phase behavior of these two systems were studied with differential scanning calorimetry. Computational studies such as the search for stable conformers, lattice-energy calculations, and Hirshfeld surface analysis were performed to shed light on the polymorphism, relative stability of the forms in each system, and contribution of intermolecular interactions to the overall stability of the systems. The study confirmed the effect of substituent size on the polymorphism of the compounds.

1. INTRODUCTION

Fenamic acids (FAs) are potential nonsteroidal anti-inflammatory drugs (NSAIDs), and indeed some FAs such as mefenamic acid (MFA), tolfenamic acid (TFA), flufenamic acid (FFA), and meclofenamic acid are classic NSAIDs on the market.[1−3] FAs possess intrinsic conformational flexibility. Intuitively, these compounds are prone to crystallize in different forms, i.e., polymorphs. In practice, several FAs are found to exhibit multiple forms. For example, MFA, TFA, and FFA, have two, five, and nine known forms, respectively.[4−6] The discovery of nine forms of FFA,[7] all structurally characterized by single-crystal X-ray diffraction, is believed to be the current world record for most forms for a given compound, exceeding the previous record of eight forms for ROY.[8] Recently, 2-((2,6-dimethylphenyl)amino)benzoic acid (HDMPA)[9] and 4-chloro-2-phenylanthranilic acid (CPAA)[10] were found to be polymorphic. In particular, halogen bonding seems to have played an important role in the polymorphism of the latter. The polymorphism of FAs is mainly attributed to their conformational flexibility and sometimes the participation of other weak intermolecular interactions.[11,12] The isosteric compounds of FAs, i.e., phenylaminonicotinic acids (PNAs),

Received: December 23, 2018
Revised: April 9, 2019
Published: April 10, 2019

DOI: 10.1021/acs.cgd.8b01902
Cryst. Growth Des. 2019, 19, 3694−3703

are also prone to exist in multiple forms in the solid state, as suggested by the polymorphism of a series of compounds including clonixin (CLX),[13] niflumic acid (NFA),[14,15] 2-phenylaminonicotinic acid (2-PNA),[16−18] 2-(methyl-phenyl-amino)-nicotinic acid (2-MPNA),[19] and other compounds,[20,21] due to both conformational flexibility and synthon variation (Scheme 1). Recently, CLX was found to form

Scheme 1. Representative Polymorphic FAs and PNAs

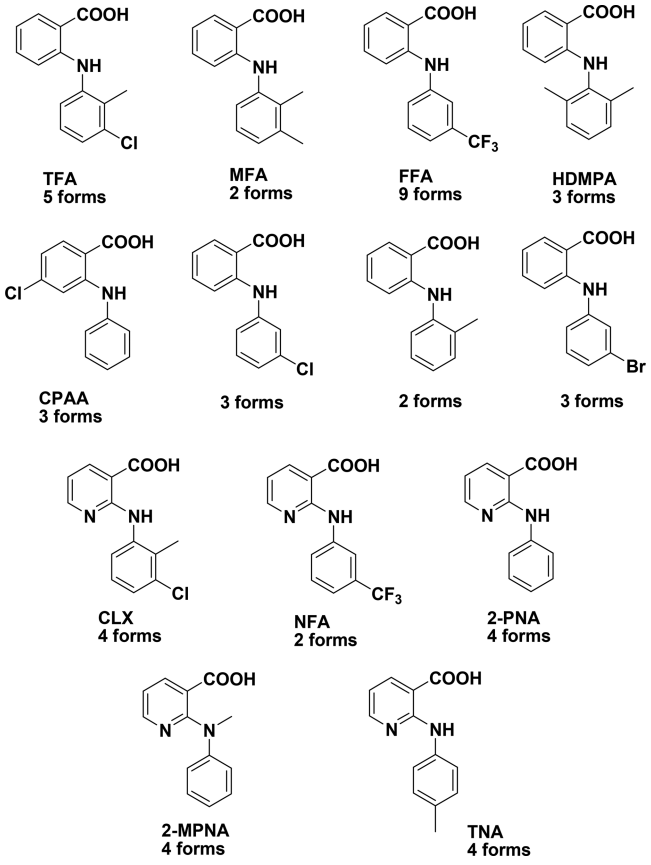

solvates with *N*,*N*-dimethylformamide and its analogues.[22,23] Polymorphism as a phenomenon is widely observed in molecular compounds and is of particular significance in pharmaceuticals because different forms of the same active pharmaceutical ingredient (API) may have different properties, e.g., kinetic, thermodynamic, surface, mechanical, and packaging, which can affect clinical formulation and eventual bioavailability. Meanwhile, polymorphism is also important theoretically, as demonstrated by a series of crystal structure prediction (CSP) tests.[24,25,26]

Although many FAs exhibit polymorphism, the parent compound, fenamic acid, has only one modification found so far, despite extensive polymorph screening. Obviously, substitution leads to multiple forms in its analogues. In a novel study, Matzger and co-workers attempted to identify the polymorphophore (structure moiety contributing to polymorphism of a given compound) for FAs, and their conclusion was that substitution on the aniline ring acted as polymorphophore.[27] In this study, we wanted to explore whether substituent size and isomerization were also factors. By substituting the benzene with naphthalene, we synthesized 2-(naphthalen-1-ylamino)-benzoic acid and 2-(naphthalen-2-ylamino)-benzoic acid and investigated their polymorphism (Scheme 2).

Scheme 2

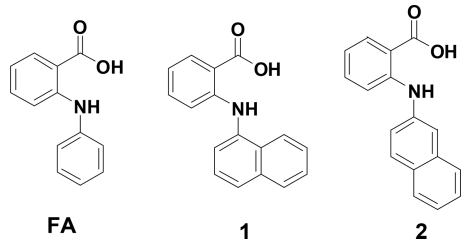

As can be seen, the only difference between FA and compound **1** is the overall size of the two compounds due to switching the benzene ring in FA to naphthalene in **1**, which could change the steric interaction between the two aromatic moieties of the compound and potential intermolecular interactions. And for compounds **1** and **2**, the difference lies in the position of the amino group on the naphthalene ring, and intuitively, the two compounds should behave similarly.

2. EXPERIMENTAL SECTION

2.1. Materials. All chemicals were purchased from commercial sources. 2-Chlorobenzoic acid and naphthalene-1-amine were from Shanghai Aladdin Biochemical Technology Co., Ltd. (Shanghai, China); naphthalene-2-amine was from Energy Chemical Co., Ltd. (Shanghai, China); 2-ethoxyethanol was from J&K Scientific Ltd. (Beijing, China); copper powder and copper oxide powder were from Tianjin Heowns Biochemical Technology Co., Ltd. (Tianjin, China); potassium carbonate and other organic solvents were from Sinopharm Chemical Reagent Co., Ltd. (Shanghai, China) and were used as received.

2.2. Synthesis. Literature procedures were followed to synthesize NBAs (Scheme 3).[28,29] Synthetic details can be found in the Supporting Information (SI).

2.3. Crystal Growth. Crystallization trials were conducted using previously established protocols[23] using a series of common organic solvents (see Table 1) because the synthesized NBAs are known to be largely insoluble in aqueous media. Single crystals of each compound were obtained under ambient conditions by slow evaporation of saturated solutions. A typical set up entailed dissolution of ∼50 mg of NBA (i.e., **1** or **2**) in ∼10 mL of HPLC-grade solvent in glass sample vials. The rate of evaporation was controlled (retarded) by covering the vials with perforated Parafilm. Crystals suitable for X-ray diffraction analysis formed over several days. Owing to differing solvent volatility, some trials had evaporated to yield dry crystals, while others were still wet in their mother liquor.[30]

2.4. Crystal Structure Determination. Crystal structures for each of the polymorphs were determined by single-crystal X-ray diffraction using procedures similar to those in our recent work on Clonixin.[23] For **1-I**, **1-II**, and **2-I**, data collection was performed on a Nonius kappaCCD diffractometer at low temperature (90 K) using Mo Kα X-rays (λ = 0.71073 Å),[31] while data for **2-II** were obtained on a Rigaku-Oxford Diffraction Excalibur diffractometer at room temperature (293 K) with Cu Kα X-rays (λ = 1.54178 Å). Data processing (indexing, integration, scaling and merging) was done with Denzo-SMN and ScalePack (**1-I**, **1-II**, **2-I**), and by CrysAlisPro (**2-II**). Structures were solved using SHELXS and refined with SHELXL.[32,33]

For powder X-ray diffraction (PXRD), samples were finely pulverized and placed in an aluminum holder on quartz plates. Powder patterns were recorded on a Rigaku X-ray diffractometer with Cu Kα_1 (1.5406 Å; 40 kV, 40 mA) at ambient temperature.

2.5. Thermal Analyses. Differential scanning calorimetry (DSC) experiments were performed on TA Instruments DSCQ20-1250 to

DOI: 10.1021/acs.cgd.8b01902
Cryst. Growth Des. 2019, 19, 3694−3703

Scheme 3. Synthesis of NBAs

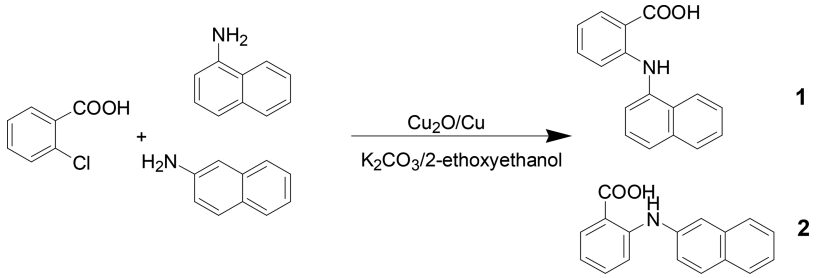

Table 1. Crystal Growth Conditions of Compounds 1 and 2

solvent	method	form	form
ethyl acetate	slow evaporation	**1-I**	**2-I**
methanol	slow evaporation	**1-II**	**2-I**
dichloromethane	slow evaporation	**1-I**	**2-I**
ethanol	slow evaporation	**1-II**	**2-I**
acetonitrile	slow evaporation	**1-I**	**2-II**
ether	slow evaporation	**1-I**	**2-I**
tetrahydrofuran	slow evaporation	**1-I**	**2-I**
acetone	slow evaporation	**1-I**	**2-I**
chloroform	slow evaporation	**1-I**	**2-I**
isopropanol	slow evaporation	**1-II**	**2-I**
dimethyl sulfoxide	slow evaporation	**1-I**	**2-I**
acetic acid	slow evaporation	**1-I**	**2-I**
N,*N*-dimethylformamide	slow evaporation	**N/A**	**2-I**
benzene	slow evaporation	**1-I**	**2-I**
toluene	slow evaporation	**1-I**	**2-I**
pet ether	slow evaporation	**N/A**	**N/A**
hexane	slow evaporation	**N/A**	**N/A**
water	slow evaporation	**N/A**	**N/A**

study the phase behavior of the solid forms. The procedure is the same as the one used before.[23]

2.6. Spectroscopic Measurement. IR and Raman spectra were recorded using a PerkinElmer FT-IR spectrometer and a Thermo Raman confocal microscope, respectively. A literature procedure was applied.[23]

2.7. Computational Studies. We conducted a series of quantum mechanics calculations to investigate the potential factors influencing the polymorphism.[23] First, molecular conformations were optimized and scanned for comparison. Then, crystal structures were optimized for lattice-energy estimation of NBAs. Meanwhile, molecular packing modes were examined by Hirshfeld surface analyses.[3435]

All molecular conformations were optimized at the B3LYP/6-311g(d,p)[3637] level based on their crystal structures. Frequency calculations were performed at the same level to identify the minima (zero imaginary frequency), except for the assumed planar conformations. The potential energy surface scan of dihedral angle C1N7C8C9 was conducted in steps of 10 deg at the same level.

Crystal structures were first optimized at the PW1PW/6-21g-(d,p)[38] level with the experimental lattice parameters with Crystal14.[39] Contributions of dispersion energy were calculated with the DFT-D3 program of Grimme with Becke-Johnson damping.[4041] During the calculations, basis set superposition error (BSSE) was also included. Convergence criteria were set to the defaults of Crystal14.

3. RESULTS AND DISCUSSION

3.1. Crystal Structures. For each of compounds **1** and **2**, two polymorphs were discovered (Figure 1). **1-I** crystals were obtained as red needles, from ethyl acetate (EtOAc), tetrahydrofuran (THF), dichloromethane (DCM), ether (Et_2O), chloroform ($CHCl_3$), acetonitrile (CH_3CN), dimethyl sulfoxide (DMSO), benzene, toluene, acetone (CH_3COCH_3), acetic acid, or toluene; **1-II** crystals were grown as light red plates from methanol (MeOH), ethanol (EtOH), or isopropanol; **2-I** crystals were harvested as red blocks from ether, benzene, DMF, DMSO, DCM, THF, toluene, $CHCl_3$, acetic acid, acetone, EtOH, isopropanol, EtOAc, or MeOH, and **2-II** crystals as red blocks from CH_3CN.

Table 1 summarizes the crystallization results. Forms **1-I**, **1-II**, **2-I**, and **2-II** are monoclinic, space groups *C*2/c, $P2_1/c$, *C*2/*c*, and $P2_1/c$, respectively. Table 2 lists the crystallographic data of the forms.

The two molecules in the asymmetric unit of forms **1-I** and **1-II** are conformers with different dihedral angles between the two aromatic rings (53.70 (7)° in **1-I** and 88.12 (5)° in **1-II**). Similar conformers can be observed in the polymorphs of compound **2** (60.52 (5)° in **2-I** and 63.23(4)° in **2-II**). Major conformational differences in **1** and similarity in **2** can be seen by the superposition of the molecules in the corresponding forms (Figure 2).

The asymmetric unit of all crystal forms contains one molecule ($Z' = 1$). In **1-I**, the molecule is nonplanar, forming the acid−acid dimer homosynthon ($R_2^2(8)$ in graph set notation,[424344] Figures 3 and 4) with the bond length and angle of 1.819 (2.654) Å and 171.98°, respectively. The **1-II** molecule also has a nonplanar conformation with its aromatic rings nearly perpendicular to each other. These molecules also form acid−acid dimers (Figures 3 and 4), with the hydrogen-bond parameters being 1.799 (2.638) Å and 175.64°, respectively. In addition, in both forms the NH bridging the two aromatic rings and the carbonyl O (S6) form an intramolecular hydrogen bond. The bond distance and angle are 1.926 (2.637) Å and 136.61° in **1-I** and 2.007 (2.680) Å and 132.38° in **1-II**.

Similar observations are made for compound **2**. A highly twisted molecule with the aforementioned dihedral angle of 60.52 (5)° is in the asymmetric unit of **2-I**. The molecules are connected through the acid−acid homosynthon ($R_2^2(8)$). Here, hydrogen-bond parameters are 1.797 (2.635) Å and 175.03° intermolecularly, and 2.003(2.667) Å and 131.28° intramolecularly (Figures 3 and 4). **2-I** resembles form **1-I**. **2-II** molecule has a dihedral angle similar to that of **2-I** of 63.23(4)°, and the molecules associate through the acid−acid dimer. The bond parameters of the inter- and intramolecular hydrogen bonds are 1.872(2.689) Å and 174.50°, and 2.051(2.705) Å and 132.14°, respectively (Figure 4). Although the molecule in **2-II** is not conformationally similar to that of **1-II**, the two crystal structures have the same space group; thus **2-II** resembles **1-II**.

Figure 5 shows the PXRD patterns of individual forms of each system along with those calculated from the single-crystal

DOI: 10.1021/acs.cgd.8b01902
Cryst. Growth Des. 2019, 19, 3694−3703

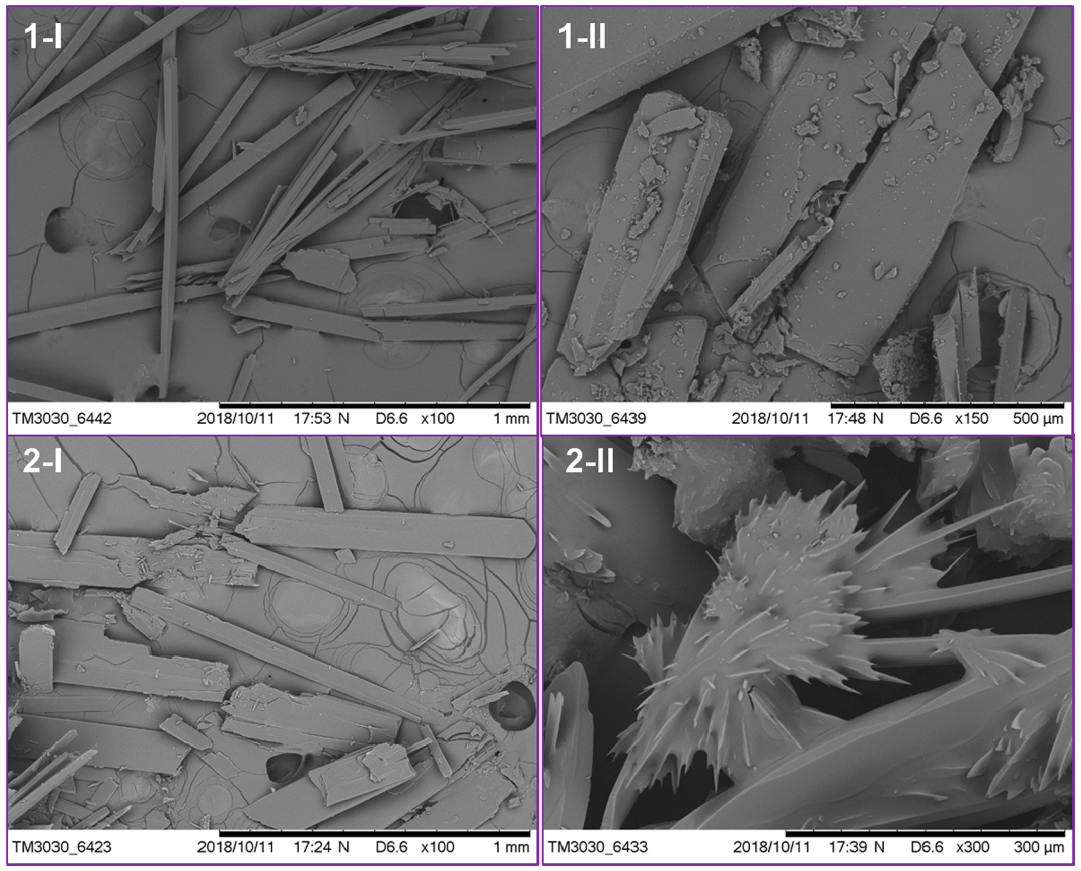

Figure 1. SEM micrographs of crystals of the polymorphs of NBAs.

Table 2. Crystallographic Data of Compounds 1 and 2

	1-I	1-II	2-I	2-II
formula	$C_{17}H_{13}NO_2$	$C_{17}H_{13}NO_2$	$C_{17}H_{13}NO_2$	$C_{17}H_{13}NO_2$
formula weight	263.28	263.28	263.28	263.28
crystal size (mm)	0.30 × 0.30 × 0.03	0.40 × 0.20 × 0.03	0.50 × 0.20 × 0.05	0.40 × 0.10 × 0.10
crystal system	monoclinic	monoclinic	monoclinic	monoclinic
space group	$C2/c$	$P2_1/c$	$C2/c$	$P2_1/c$
a/Å	11.5398(3)	12.3702(2)	23.3080(4)	12.4726(3)
b/Å	7.4605(2)	4.85480(10)	5.79720(10)	7.09820(10)
c/Å	30.2758(9)	21.7269(5)	20.0035(4)	16.7767(5)
α/°	90	90	90	90
β/°	91.4684(12)	103.7480(10)	104.8401(9)	121.472(2)
γ/°	90	90	90	90
Z, Z'	8, 1	4, 1	8, 1	4, 1
V/Å^3	2605.67(12)	1267.42(4)	2612.74(8)	1266.80(6)
D_{cal}/g cm^{-3}	1.342	1.380	1.339	1.380
T/K	90.0(2)	90.0(2)	90.0(2)	293(2)
abs coeff (mm^{-1})	0.088	0.091	0.088	0.732
F(000)	1104	552	1104	552
θ range (deg)	1.35−27.49	1.69−27.50	1.0−27.5	3.65−66.51
limiting indices	$-14 \le h \le 14$	$-16 \le h \le 16$	$-29 \le h \le 30$	$-14 \le h \le 12$
	$-9 \le k \le 9$	$-6 \le k \le 6$	$-7 \le k \le 7$	$-8 \le k \le 8$
	$-39 \le l \le 39$	$-28 \le l \le 28$	$-25 \le l \le 25$	$-17 \le l \le 17$
completeness (%)	100	100	99.9	99.9
unique reflections	1607	1655	2020	1924
R_1 [$I > 2\sigma(I)$]	0.0544	0.0536	0.0522	0.0324
wR_2 (all data)	0.1659	0.1497	0.1568	0.0914

structures. The experimental and simulated PXRD patterns show clear similarity.

3.2. Thermal Properties. Phase behavior study of each form by DSC revealed a single thermal event for **1-I** with an

DOI: 10.1021/acs.cgd.8b01902
Cryst. Growth Des. 2019, 19, 3694−3703

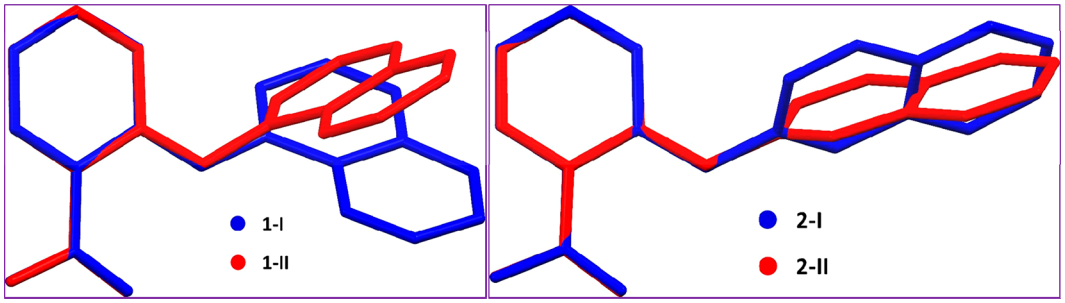

Figure 2. Superposition of the molecules in the asymmetric units of compounds **1** and **2** polymorphs.

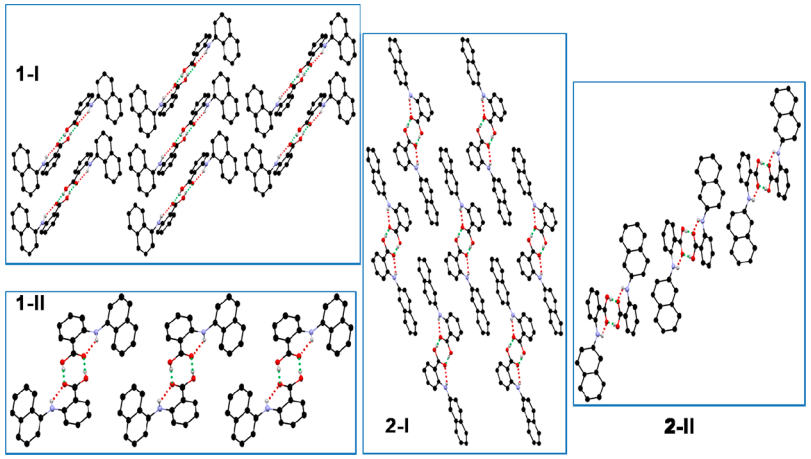

Figure 3. Crystal packing of **1-I**, **1-II**, **2-I**, and **2-II**. For clarity, only hydrogens participating hydrogen bonds are shown.

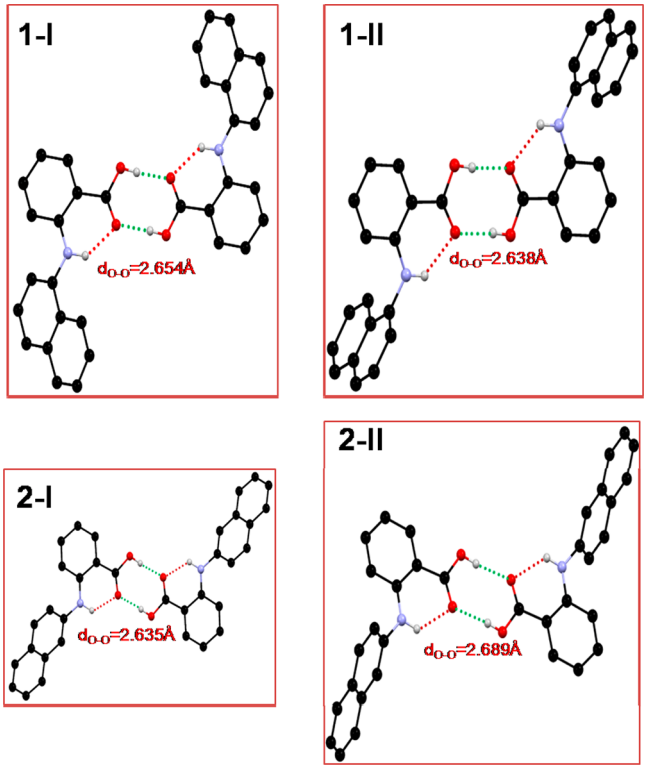

Figure 4. Hydrogen-bonding dimer in **1-I**, **1-II**, **2-I**, and **2-II**. For clarity, only hydrogens participating hydrogen bonds are shown.

onset temperature of 207 °C, which corresponds to melting (Figure 6). **1-II** showed two thermal events, with the first with an onset temperature of 162 °C, corresponding to the phase transition to **1-I**, followed by melting of **1-I**, as suggested by a 207 °C onset temperature (Figure 6a). **2-I** revealed only one thermal event with an onset temperature of 209 °C, corresponding to melting of the crystals. **2-II** displayed two thermal events with the first one at 118 °C, which is a solid–solid phase transition into **2-I**, which melted at 211 °C (Figure 6b).

3.3. Computational Analyses. Single (isolated) molecules optimization indicates that the twisted conformers are more stable than planar conformers, and imaginary frequencies were found for the assumed planar structures with *Cs* symmetry. This is not surprising in light of the huge steric hindrance from the naphthyl substituent. The energy differences span 2–6 kcal/mol (Table 3). Similarly, the twisted conformer is more stable than the planar one in FA, as the latter has a relative Gibbs free energy of 3.56 kcal/mol.

For compound **1**, there are two minimal twisted conformations with an energy difference of only about 1 kcal/mol. For compound **2**, there are also two minimal twisted conformations, with almost the same energies. Major conformational difference stems from the dihedral angle of the two aromatic rings, as illustrated by Figures 7 and 8. Conformation energy scan of compounds **1** and **2** (Figures 7 and 8) shows similar results, as suggested by the two local minima and energy barriers.

In contrast, the conformational scan for FA revealed one global minimum and one symmetrical minimum.[45] The two conformations in the only crystal structure obtained so far through a thorough polymorph screening lie in the global minimum energy well, and they should be considered as conformational adjustment instead of conformational

DOI: 10.1021/acs.cgd.8b01902
Cryst. Growth Des. 2019, 19, 3694–3703

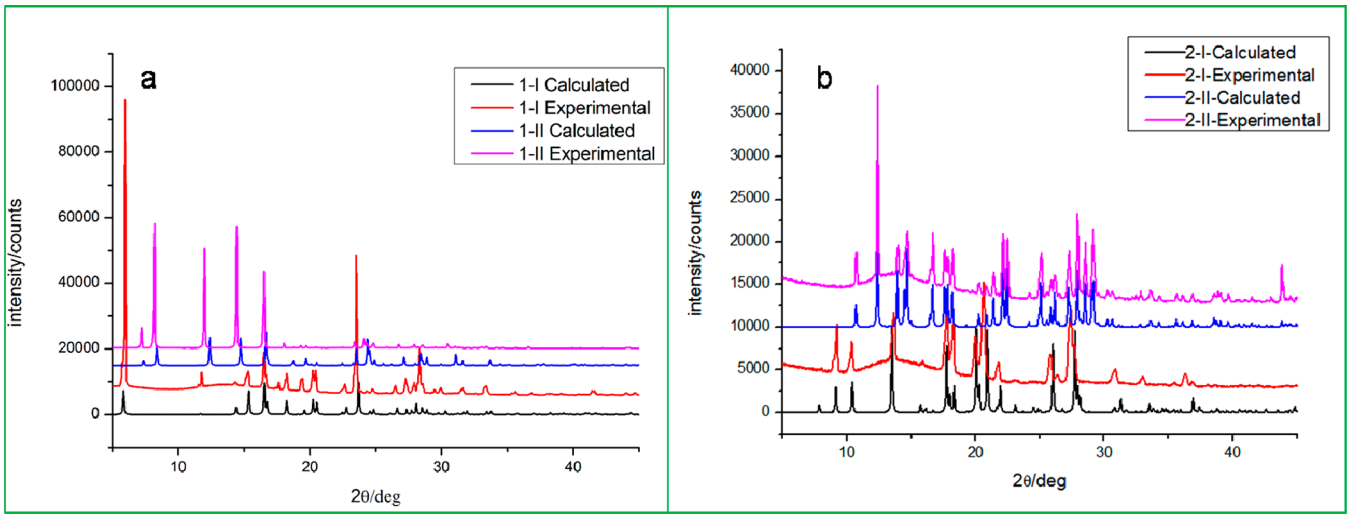

Figure 5. PXRD patterns of polymorphs of compounds **1** (a) and **2** (b).

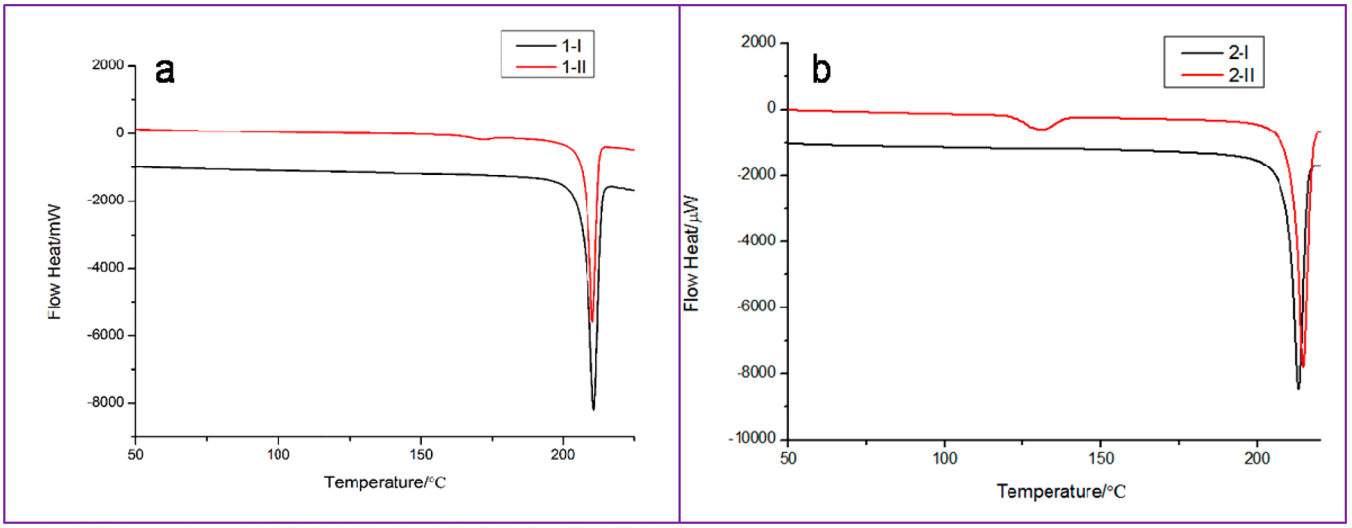

Figure 6. DSC thermograms of compounds **1** (a) and **2** (b) polymorphs.

Table 3. Relative Energies between Twisted and Planar Conformations of Compounds 1 and 2[a]

	torsion angle	*E* (Hartree)	Δ*E* (kcal/mol)	*G* (Hartree)	Δ*G* (kcal/mol)
1-twisted-1	41.9	−861.094484	0.00	−860.878596	0.00
1-twisted-2	105.1	−861.092675	1.13	−860.877775	0.52
1-planar-1	0.0	−861.087071	4.65	−860.868628	6.26
2-twisted-1	32.1	−861.095702	0.00	−860.880081	0.00
2-twisted-2	142.2	−861.095558	0.09	−860.880065	0.01
2-planar-1	0.0	−861.092061	2.28	−860.874995	3.19
2-planar-2	180.0	−861.090102	3.51	−860.873202	4.32

[a]Gibbs free energies were calculated under 298.15 K and 1 atm.

change.[46] According to the studies by Price et al. and Matzger et al., the lack of polymorphs for FA lies in the fact that the known and a closely related hypothetical structure are thermodynamically favored over other calculated ones, limiting the range of potential polymorphism.

The lattice energies of the two forms of compounds **1** and **2** were calculated to be −54.75, −52.23, −54.48, and −52.59 kcal/mol for **1-I**, **1-II**, **2-I**, and **2-II**, respectively. It can be inferred that for both systems, form **I** is more stable than form **II**. This is supported by the DSC studies since **1-II** converts into **1-I** and **2-II** into **2-I** under thermal treatment, which indicates the relative stability order is **1-I** > **1-II** and **2-I** > **2-II**.

Hirshfeld surface analysis[34] provides us a better understanding of the molecular interactions in the crystals. The relative contributions of various intermolecular interactions were calculated by CrystalExplore.[47] In **1-I**, the dominant interactions, coded by the bright red in Figure 9, are caused by hydrogen bonds between the carboxylic acids, and it accounts for 12.1% of the overall Hirshfeld surface. This dominant interaction is also represented by two spikes in the left-bottom

DOI: 10.1021/acs.cgd.8b01902
Cryst. Growth Des. 2019, 19, 3694−3703

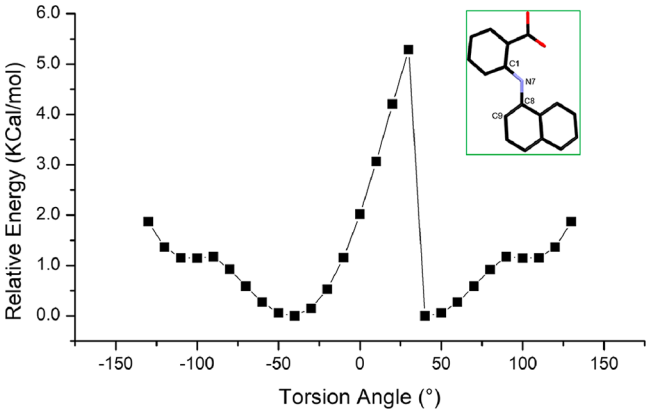

Figure 7. Relaxed potential energy surface (PES) scan for the N7−C8 bond of compound **1**.

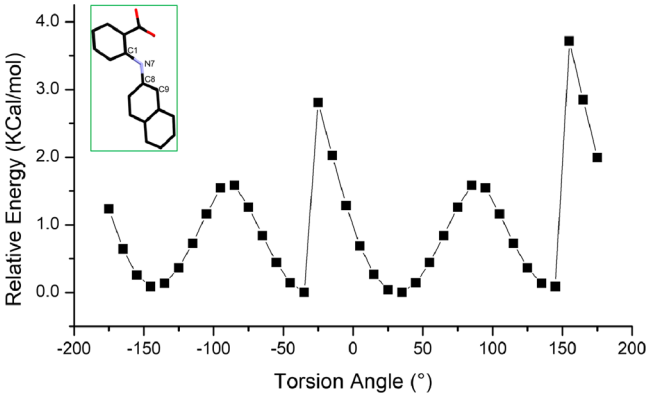

Figure 8. Relaxed potential energy surface (PES) scan for the N7−C8 bond of compound **2**.

region of the fingerprint plot in Figure 10. Other close contacts (interactions) were also counted with their contributions to the Hirshfeld surface area in Figure 11. A weak H-π interaction embodied by C···H contacts occupies 36.8% of the Hirshfeld surface. H−H contacts take 44.3% of the Hirshfeld surface. The parallel packing mode of the benzoic acid dimers with $\pi\cdots\pi$ stacking interaction is represented in C···C and C···O contacts with a proportion of about 3%. The molecular interactions in **1-II** are similar to those in **1-I**, but the parallel packing mode of the benzoic acid part gives a different slipped shift, and the torsion angle of the two aromatic rings in **1-II** is larger than that in **1-I**, so that obvious differences in the fingerprint plot can be found, as indicated by the corresponding major intermolecular contacts being 10.2%, 25.6%, 52.3%, 7.2%, and 3.5%, respectively, of the Hirshfeld surface (Figure 10).

Compound **2** shows very similar packing modes to compound **1**, with **2-I** closely resembling **1-I** and **2-II** being like **1-II**, which verified the similarity between the molecular and crystal structures. Hydrogen-bond interactions and $\pi-\pi$ and H−π interactions can all be found in **2-I** and **2-II**, and the different torsion angles of the aromatic rings and the slipped parallel packing modes of the benzoic acid parts can also be found between **2-I** and **2-II**. Their similar Hirshfeld surfaces and different fingerprint plots are also given in Figures 9, 10, and 11.

In addition, the hydrogen-bond dimer of each compound can be sketched like the pattern in Figure 12a, in which "a" means the carboxyl acid part, "b" means the benzene ring part, and "n" means the naphthyl part. Two packing modes are shown in Figure 12b,c, with different slipped parallel packing modes for **1-I** and **1-II**.

4. CONCLUSIONS

Two NBAs were synthesized by replacing the benzene ring in FA with naphthalene in NBAs, and investigation of their polymorphism was undertaken. Two forms were discovered for each compound. Similar to FA, acid−acid dimer homosynthon is the structural motif in the crystals, regardless of the dihedral angle between the two aromatic rings. **1-I** and **2-I**, and **1-II** and **2-II** showed structural similarity, which indicates that substituent size plays a significant role in the polymorphism,

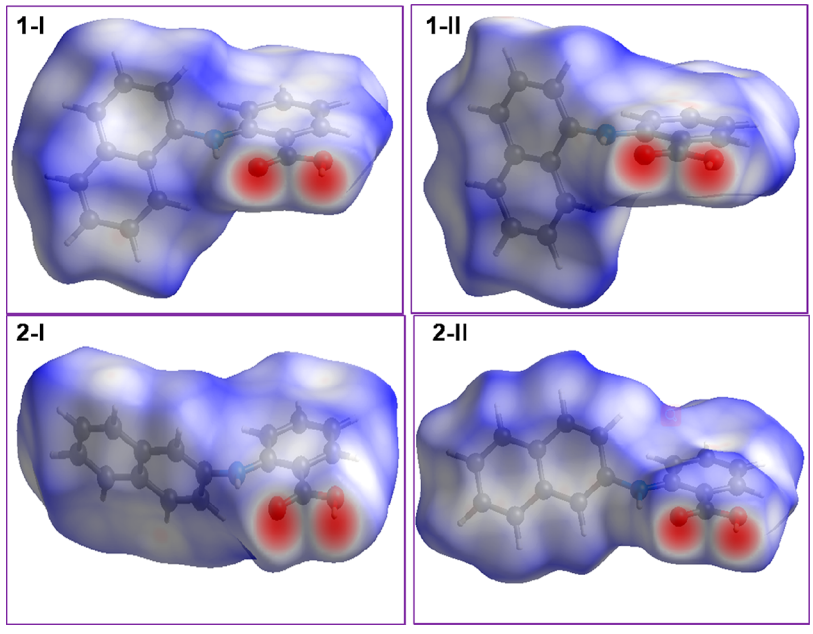

Figure 9. Hirshfeld surfaces of the polymorphs of compounds **1** and **2**.

DOI: 10.1021/acs.cgd.8b01902
Cryst. Growth Des. 2019, 19, 3694−3703

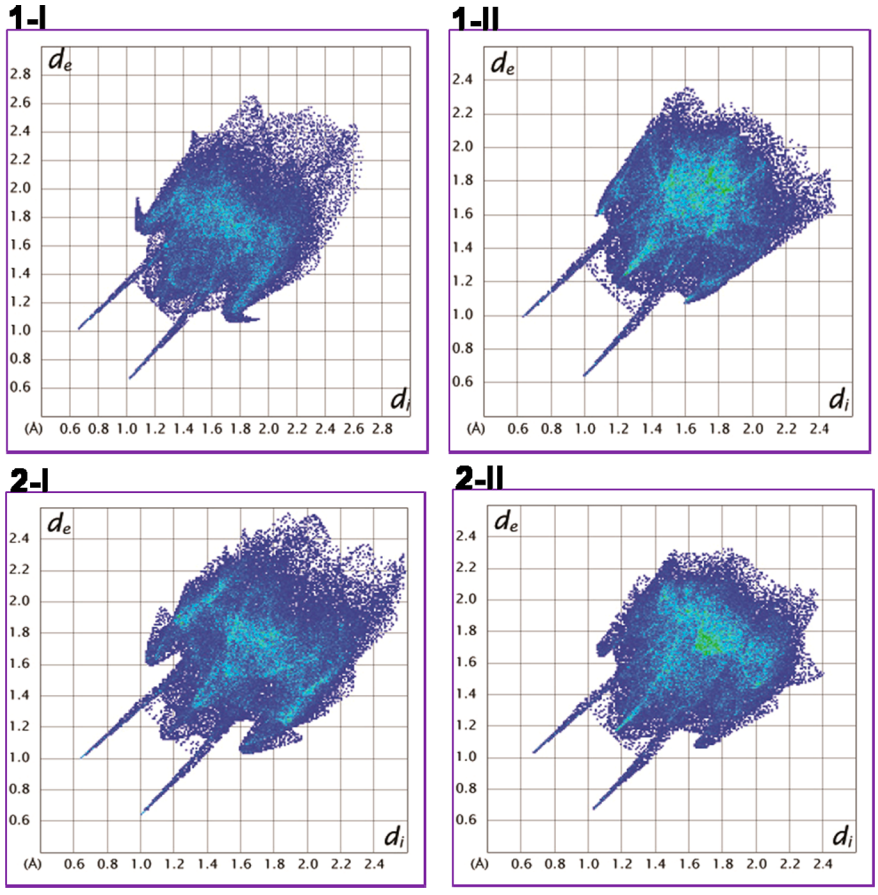

Figure 10. Fingerprint plots of the Hirshfeld surface area of the polymorphs of compounds **1** and **2**.

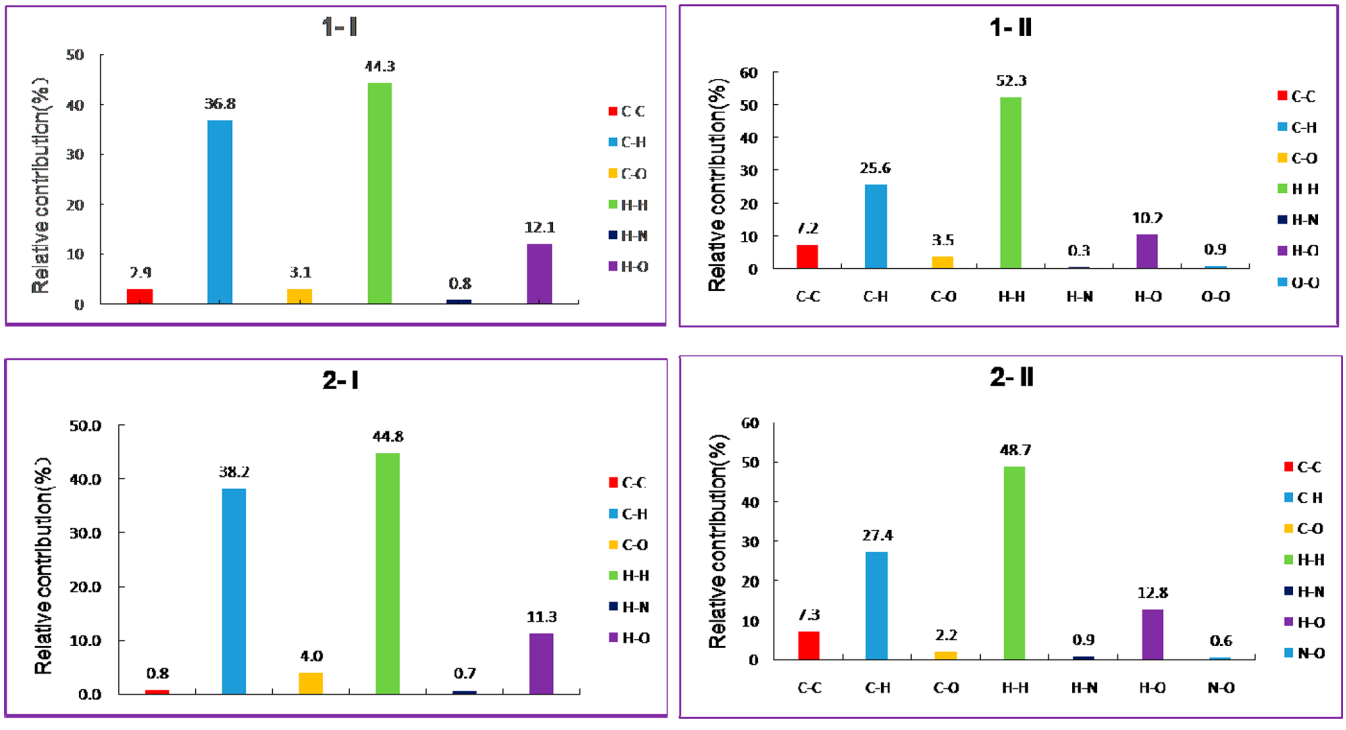

Figure 11. Relative contributions of different intermolecular contacts to the Hirshfeld surface area of the polymorphs of compounds **1** and **2**.

and isomerization only leads to variation in cell parameters. A phase behavior study of the two polymorphic systems by DSC showed both **1-II** and **2-II** transformed into **1-I** and **2-I**, respectively. Conformational energy evaluations and conformation scans suggested that due to the increase of the substituent size, the two compounds exhibit both conforma-

DOI: 10.1021/acs.cgd.8b01902
Cryst. Growth Des. 2019, 19, 3694−3703

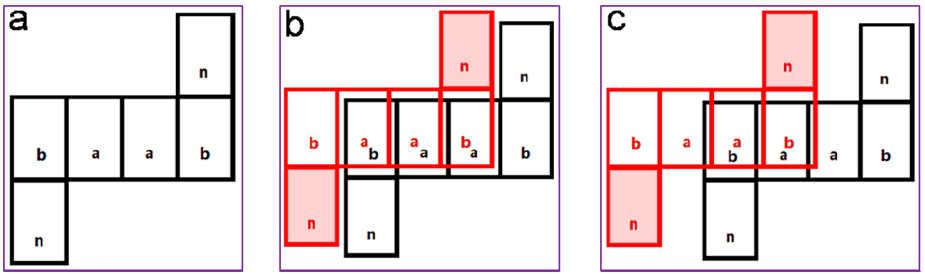

Figure 12. (a–c) Sketch maps of the hydrogen-bond dimers and their packing modes.

tional flexibility and rigidity, which together with other factors are responsible for the polymorphism of the compounds. Considering the concept of polymorphophore proposed by Matzger, naphthalene can be regarded as disubstituted benzene which should also be considered as a polymorphophore, leading to the polymorphism of both compounds. Computational studies such as lattice-energy comparison and Hirshfeld surface analysis further shed light on the relative stability of each polymorph and the contribution of individual intermolecular interactions to the stability of each form.

■ ASSOCIATED CONTENT

Supporting Information

The Supporting Information is available free of charge on the ACS Publications website at DOI: 10.1021/acs.cgd.8b01902.

Synthesis of NBAs, Figure S1: IR spectra of the two polymorphs of compound **1**, Figure S2: IR spectra of the two polymorphs of compound **2**, Figure S3: Raman spectra of the two polymorphs of compound **1**, Figure S4: Raman spectra of the two polymorphs of compound **2** (PDF)

Accession Codes

CCDC 1885343–1885346 (four crystal structures of the two compounds) contain the supplementary crystallographic data for this paper. These data can be obtained free of charge via www.ccdc.cam.ac.uk/data_request/cif, or by emailing data_request@ccdc.cam.ac.uk, or by contacting The Cambridge Crystallographic Data Centre, 12 Union Road, Cambridge CB2 1EZ, UK; fax: +44 1223 336033.

■ AUTHOR INFORMATION

Corresponding Authors

*(F.Y.) Phone: (027) 87194980. E-mail: fyuwucn@gmail.com.
*(S.L.) E-mail: Sihuilong@wit.edu.cn, longsihui@yahoo.com.

ORCID

Tonglei Li: 0000-0003-2491-0263
Conggang Li: 0000-0002-5798-1722
Faquan Yu: 0000-0002-5062-8731
Sihui Long: 0000-0002-4424-6374

Notes

The authors declare no competing financial interest.

■ ACKNOWLEDGMENTS

S.L. thanks Natural Science Foundation of Hubei Province for financial support (2014CFB787). Y.L. thanks the sponsorship from Innovation Fund of the Graduate School (CX2018022). T.L. is grateful to NSF for supporting the work (DMR1006364). S.R.P. is grateful to the NSF MRI Program (CHE0319176 and CHE1625732).

■ REFERENCES

(1) Jabeen, S.; Dines, T. J.; Leharne, S. A.; Chowdhry, B. Z. Raman and IR spectroscopic studies of fenamates-Conformational differences in polymorphs of flufenamic acid, mefenamic acid and tolfenamic acid. *Spectrochim. Acta, Part A* **2012**, *96*, 972–985.

(2) Bouanga Boudiombo, J. S.; Jacobs, A. Solvates of selected fenamic acids with substituted pyridines: structure, thermal stability and desolvation. *Acta Crystallogr., Sect. B: Struct. Sci., Cryst. Eng. Mater.* **2016**, *72*, 836–845.

(3) Sanphui, P.; Bolla, G.; Nangia, A. High Solubility Piperazine Salts of the Nonsteroidal Anti-Inflammatory Drug (NSAID) Meclofenamic Acid. *Cryst. Growth Des.* **2012**, *12*, 2023–2036.

(4) Cunha, V. R. R.; Izumi, C. M. S.; Petersen, P. A. D.; Magalhães, A.; Temperini, M. L. A.; Petrilli, H. M.; Constantino, V. R. L. Mefenamic Acid Anti-Inflammatory Drug: Probing Its Polymorphs by Vibrational (IR and Raman) and Solid-State NMR Spectroscopies. *J. Phys. Chem. B* **2014**, *118*, 4333–4344.

(5) López-Mejías, V.; Kampf, J. W.; Matzger, A. J. Polymer-Induced Heteronucleation of Tolfenamic Acid: Structural Investigation of a Pentamorph. *J. Am. Chem. Soc.* **2009**, *131*, 4554–4555.

(6) López-Mejías, V.; Kampf, J. W.; Matzger, A. J. Nonamorphism in Flufenamic Acid and a New Record for a Polymorphic Compound with Solved Structures. *J. Am. Chem. Soc.* **2012**, *134*, 9872–9875.

(7) Delaney, S. P.; Smith, T. M.; Pan, D.; Yin, S. X.; Korter, T. M. Low-Temperature Phase Transition in Crystalline Aripiprazole Leads to an Eighth Polymorph. *Cryst. Growth Des.* **2014**, *14*, 5004–5010.

(8) Tan, M.; Shtukenberg, A. G.; Zhu, S.; Xu, W.; Dooryhee, E.; Nichols, S. M.; Zhu, Q.; Ward, M. D.; Kahr, B. ROY revisited, again: the eighth solved structure. *Faraday Discuss.* **2018**, *211*, 477–491.

(9) Hu, R.; Zhoujin, Y.; Liu, M.; Zhang, M.; Parkin, S.; Zhou, P.; Long, S.; Wang, J.; Yu, S. Solution growth and thermal treatment of crystals lead to two new forms of 2-((2,6-dimethylphenyl)amino)-benzoic acid. *RSC Adv.* **2018**, *8*, 15459–15470.

(10) Liu, M.; Yin, C.; Chen, P.; Zhang, M.; Parkin, S.; Zhou, P.; Long, S.; Li, F.; Yu, S. $^{sp^2}$CH···Cl hydrogen bond in the conformational polymorphism of 4-chloro-phenylanthranilic acid. *CrystEngComm* **2017**, *19*, 4345–4354.

(11) Jerzykiewicz, L.; Sroka, A.; Majerz, I. The Crystal Structure and Behavior of Fenamic Acid-Acridine Complex Under High Pressure. *J. Pharm. Sci.* **2016**, *105*, 3487–3495.

(12) Yang, F.; Yan, C. X.; Yang, X.; Zhou, D. G.; Zhou, P. P. Fenamic acid crystal with two asymmetric units (Z'=2): why Z'=2 rather than Z'=1. *CrystEngComm* **2017**, *19*, 1762–1770.

(13) Takasuka, M.; Nakai, H.; Shiro, M. Infrared spectral and X-ray studies of polymorphic forms of 2-(2-methyl-3-chloroanilino)-nicotinic acid. *J. Chem. Soc., Perkin Trans. 2* **1982**, *2*, 1061–1067.

(14) Bag, P. P.; Reddy, C. M. Screening and Selective Preparation of Polymorphs by Fast Evaporation Method: A Case Study of Aspirin, Anthranilic Acid, and Niflumic Acid. *Cryst. Growth Des.* **2012**, *12*, 2740–2743.

(15) Romero, S.; Bustamante, P.; Escalera, B.; Cirri, M.; Mura, P. Characterization of the solid phases of paracetamol and fenamates at equilibrium in saturated solutions. *J. Therm. Anal. Calorim.* **2004**, *77*, 541–554.

DOI: 10.1021/acs.cgd.8b01902
Cryst. Growth Des. 2019, 19, 3694–3703

(16) Long, S.; Parkin, S.; Siegler, M. A.; Cammers, A.; Li, T. Polymorphism and Phase Behaviors of 2-(Phenylamino)nicotinic Acid. *Cryst. Growth Des.* **2008**, *8*, 4006−4013.
(17) Kalra, A.; Lubach, J. W.; Munson, E. J.; Li, T. Exploring Molecular Speciation and Crystallization Mechanism of Amorphous 2-Phenylamino Nicotinic Acid. *Pharm. Res.* **2018**, *35*, 1−13.
(18) Li, T.; Zhou, P.; Mattei, A. Electronic origin of pyridinyl N as a better hydrogen-bonding acceptor than carbonyl O. *CrystEngComm* **2011**, *13*, 6356−6360.
(19) Long, S.; Parkin, S.; Siegler, M.; Brock, C. P.; Cammers, A.; Li, T. Polymorphism of an Organic System Effected by the Directionality of Hydrogen-Bonding Chains. *Cryst. Growth Des.* **2008**, *8*, 3137−3140.
(20) Nath, N. K.; Kumar, S. S.; Nangia, A. Neutral and Zwitterionic Polymorphs of 2-(p-Tolylamino)nicotinic Acid. *Cryst. Growth Des.* **2011**, *11*, 4594−4605.
(21) López-Mejías, V.; Matzger, A. J. Structure-Polymorphism Study of Fenamates: Toward Developing an Understanding of the Polymorphophore. *Cryst. Growth Des.* **2015**, *15*, 3955−3962.
(22) Long, S.; Mao, T.; Chen, P.; Liu, M.; Parkin, S.; Zhang, M.; Yu, F.; Li, T.; Zhou, P. Strong Hydrogen Bond Leads to a Fifth Crystalline Form and Polymorphism of Clonixin. *Chem. Select.* **2017**, *2*, 4942−4950.
(23) Liu, M.; Shen, G.; Yuan, Z.; Parkin, S.; Yu, F.; Zhang, M.; Li, T.; Long, S. Substituent Electronegativity and Isostructurality in the Polymorphism of Clonixin Analogues. *Cryst. Growth Des.* **2018**, *18*, 7006−7014.
(24) Vasileiadis, M.; Pantelides, C. C.; Adjiman, C. S. Prediction of the crystal structures of axitinib, a polymorphic pharmaceutical molecule. *Chem. Eng. Sci.* **2015**, *121*, 60−76.
(25) Price, S. L. Is zeroth order crystal structure prediction (CSP_0) coming to maturity? What should we aim for in an ideal crystal structure prediction code? *Faraday Discuss.* **2018**, *211*, 9−30.
(26) Reilly, A. M.; Cooper, R. I.; Adjiman, C. S.; Bhattacharya, S.; Boese, A. D.; Brandenburg, J. G.; Car, R.; et al. Report on the sixth blind test of organic crystal structure prediction methods. *Acta Crystallogr., Sec. B: Strut. Sci.* **2016**, *72*, 439−459.
(27) López-Mejías, V.; Matzger, A. J. Structure-Polymorphism Study of Fenamates: Toward Developing an Understanding of the Polymorphophore. *Cryst. Growth Des.* **2015**, *15*, 3955−3962.
(28) Mei, X.; August, A. T.; Wolf, C. Regioselective Copper-Catalyzed Amination of Chlorobenzoic Acids: Synthesis and Solid-State Structures of N-Aryl Anthranilic Acid Derivatives. *J. Org. Chem.* **2006**, *71*, 142−149.
(29) Maradolla, M. B.; Amaravathi, M.; Kumar, V. N.; Chandra Mouli, M. G. V. P. Regioselective copper-catalyzed amination of halobenzoic acids using aromatic amines. *J. Mol. Catal. A: Chem.* **2007**, *266*, 47−49.
(30) Kumar, M. S.; Rajesh, K.; Vijayaraghavan, G. V.; Krishnan, S. Growth, structural and mechanical studies of phthalic acid single crystals grown in two different solutions. *Mater. Res. Express* **2018**, *5*, 115101.
(31) Sørensen, H. O.; Larsen, S. Measurement of high-quality diffraction data with a Nonius KappaCCD diffractometer: finding the optimal experimental parameters. *J. Appl. Crystallogr.* **2003**, *36*, 931−939.
(32) Sheldrick, G. M. A short history of SHELX. *Acta Crystallogr., Sect. A: Found. Crystallogr.* **2008**, *64*, 112−122.
(33) Sheldrick, G. M. Crystal structure refinement with SHELXL. *Acta Crystallogr., Sect. C: Struct. Chem.* **2015**, *71*, 3−8.
(34) Hirshfeld, F. L. Bonded-atom fragments for describing molecular charge densities. *Theor. Chim. Acta.* **1977**, *44*, 129−138.
(35) Spackman, M. A.; Jayatilaka, D. Hirshfeld surface analysis. *CrystEngComm* **2009**, *11*, 19−32.
(36) Becke, A. D. Density-functional thermochemistry. III. The role of exact exchange. *J. Chem. Phys.* **1993**, *98*, 5648−5652.
(37) Krishnan, R.; Binkley, J. S.; Seeger, R.; Pople, J. A. Self-consistent molecular orbital methods. XX. A basis set for correlated wave functions. *J. Chem. Phys.* **1980**, *72*, 650−654.
(38) Weigend, F.; Ahlrichs, R. Balanced basis sets of split valence, triple zeta valence and quadruple zeta valence quality for H to Rn: Design and assessment of accuracy. *Phys. Chem. Chem. Phys.* **2005**, *7*, 3297−3305.
(39) Dovesi, R.; Orlando, R.; Erba, A.; Zicovich-Wilson, C. M.; Civalleri, B.; Casassa, S.; Maschio, L.; Ferrabone, M.; De La Pierre, M.; D'Arco, P.; Noel, Y.; Causa, M.; Rerat, M.; Kirtman, B. CRYSTAL14: A program for the ab initio investigation of crystalline solids. *Int. J. Quantum Chem.* **2014**, *114*, 1287−1317.
(40) Grimme, S. Supramolecular Binding Thermodynamics by Dispersion-Corrected Density Functional Theory. *Chem. - Eur. J.* **2012**, *18*, 9955−9964.
(41) Grimme, S.; Ehrlich, S.; Goerigk, L. Effect of the damping function in dispersion corrected density functional theory. *J. Comput. Chem.* **2011**, *32*, 1456−1465.
(42) Etter, M. C. Encoding and decoding hydrogen-bond patterns of organic compounds. *Acc. Chem. Res.* **1990**, *23*, 120−126.
(43) Etter, M. C.; Macdonald, J. C.; Bernstein, J. Graph-set analysis of hydrogen-bond patterns in organic crystals. *Acta Crystallogr., Sect. B: Struct. Sci.* **1990**, *46*, 256−265.
(44) Bernstein, J.; Davis, R. E.; Shimoni, L.; Chang, N. L. Patterns in hydrogen bonding: functionality and graph set analysis in crystals. *Angew. Chem., Int. Ed. Engl.* **1995**, *34*, 1555−1573.
(45) Uzoh, O. G.; Cruz-Cabeza, A. J.; Price, S. L. Is the fenamate group a polymorphophore? Contrasting the crystal energy landscapes of fenamice and tolfenamic acids. *Cryst. Growth Des.* **2012**, *12*, 4230−4239.
(46) Cruz-Cabeza, A. J.; Bernstein, J. Conformational Polymorphism. *Chem. Rev.* **2014**, *114*, 2170−2191.
(47) Mackenzie, C. F.; Spackman, P. R.; Jayatilaka, D.; Spackman, M. A. Crystal Explorer model energies and energy frameworks: extension to metal coordination compounds, organic salts, solvates and open-shell systems. *IUCrJ* **2017**, *4*, 575−587.

DOI: 10.1021/acs.cgd.8b01902
Cryst. Growth Des. 2019, 19, 3694−3703